A bioluminescence imaging based *in vivo* model for preclinical testing of novel cellular immunotherapy strategies to improve the graft-versus-myeloma effect

Henk Rozemuller,[1] Ellen van der Spek,[2] Lijnie H. Bogers-Boer,[2] Mieke C. Zwart,[1] Vivienne Verweij,[1] Maarten Emmelot,[3] Richard W. Groen,[4] Robbert Spaapen,[3] Andries C. Bloem,[1] Henk M. Lokhorst,[2] Tuna Mutis,[3] and Anton C. Martens[1]

[1]Dept. of Immunology, [2]Haematology, [3]Clinical Chemistry and Haematology of the University Medical Center Utrecht, Utrecht, and [4]Dept. of Pathology, University of Amsterdam, Amsterdam Medical Center, Amsterdam, The Netherlands

HR and EvdS contributed equally to this work.

Acknowledgments: the authors thank Gerard Geelen and Agnes Goderie for excellent animal care, Richard Day for providing us with the GFP-LUC plasmid, Samantha Hol for the construction of the retroviral GFP-LUC vector and Ger Arkesteijn for flow sorting of the GFP-marked MM cells.

Funding: this work was supported by grants from the Dutch Program for Tissue Engineering (DPTE, project 6729), International Myeloma Foundation (IMF) and the Dutch Cancer Society (KWF).

Manuscript received October 5, 2007. Revised version arrived on January 31, 2008. Manuscript accepted March 6, 2008.

Correspondence:
Anton C. Martens, PhD,
University Medical Center Utrecht,
Dept. of Immunology KC.02.085.2,
P.O. Box 85500, 3508 AB Utrecht,
The Netherlands.
E-mail: a.martens@umcutrecht.nl

ABSTRACT

Background

The development and preclinical testing of novel immunotherapy strategies for multiple myeloma can benefit substantially from a humanized animal model that enables quantitative real-time monitoring of tumor progression. Here we have explored the feasibility of establishing such a model in immunodeficient RAG2$^{-/-}\gamma c^{-/-}$ mice, by utilizing non-invasive bioluminescent imaging for real-time monitoring of multiple myeloma cell growth.

Design and Methods

Seven multiple myeloma cell lines, marked with a green fluorescent protein firefly luciferase fusion gene, were intravenously injected into RAG2$^{-/-}\gamma c^{-/-}$ mice. Tumor localization and outgrowth was monitored by bioluminescent imaging. The sensitivity of this imaging technique was compared to that of free immumoglobulin light chain -based myeloma monitoring. Established tumors were treated with radiotherapy or with allogeneic peripheral blood mononuclear cell infusions to evaluate the application areas of the model.

Results

Five out of seven tested multiple myeloma cell lines progressed as myeloma-like tumors predominantly in the bone marrow; the two other lines showed additional growth in soft tissues. In our model bioluminescent imaging appeared superior to free light chain-based monitoring and also allowed semi-quantitative monitoring of individual foci of multiple myeloma. Tumors treated with radiotherapy showed temporary regression. However, infusion of allogeneic peripheral blood mononuclear cells resulted in the development of xenogeneic graft-versus-host-disease and a powerful cell dose-dependent graft-versus-myeloma effect, resulting in complete eradication of tumors, depending on the *in vitro* immunogenicity of the inoculated multiple myeloma cells.

Conclusions

Our results indicate that this new model allows convenient and sensitive real-time monitoring of cellular approaches for immunotherapy of multiple myeloma-like tumors with different immunogenicities. This model, therefore, allows comprehensive preclinical evaluation of novel combination therapies for multiple myeloma.

Key words: molecular imaging, bioluminescence, luciferase gene marking, cellular immunotherapy, multiple myeloma, graft versus multiple myeloma.

Citation: Rozemuller H, van der Spek E, Bogers-Boer LH, Zwart MC, Verweij V, Emmelot M, Groen RW, Spaapen R, Bloem AC, Lokhorst HM, Mutis T, and Martens AC. A bioluminescence imaging based in vivo *model for preclinical testing of novel cellular immunotherapy strategies to improve the graft-versus-myeloma effect. Haematologica 2008; 93:1049-1057.*
doi: 10.3324/haematol.12349

Introduction

Multiple myeloma (MM) is a neoplastic disease characterized by the outgrowth of monoclonal plasma cells in the bone marrow. Over the past decade, the treatment of MM has been changed significantly by the introduction of several novel agents such as bortezomib, thalidomide and lenalidomide.[1] Furthermore, with the success of non-myeloablative conditioning in reducing transplant-related mortality, allogeneic stem cell transplantation may become a realistic and attractive therapeutic option for patients with chemotherapy-resistant MM.[2] Despite these promising achievements, MM still remains incurable, indicating the need for novel combination therapies. Unfortunately, clinical testing of several potentially promising drugs in combination or not with allogeneic stem cell transplantation is cumbersome and requires large controlled studies, once again highlighting the need for useful and convenient animal models that enable preclinical testing of novel immunological and pharmacological combination therapy strategies against MM.

To date, three xenograft models of human myeloma have been developed: SCID-Hu,[3-5] NOD/SCID,[6-10] and SCID-Rab.[11] While these models offer several opportunities to test therapeutics *in vivo* against human myeloma, each of them also has reported limitations, in particular for reproducible, convenient and sensitive monitoring of cellular immunological therapies in combination with immunomodulatory agents.[12]

To develop a model that offers an optimal platform for preclinical evaluation of cellular immunotherapies, we here tested the feasibility of using immunodeficient RAG2$^{-/-}\gamma c^{-/-}$ mice for this purpose because these mice completely lack B, T and NK cells[13] and are far more suitable than NOD/SCID mice for reproducible engraftment of human T and B cells.[14,15]

To this end we transduced seven different human MM cell lines with a retroviral vector encoding a green fluorescent protein (GFP)-luciferase fusion protein and injected them in the RAG2$^{-/-}\gamma c^{-/-}$ mice. Bioluminescence imaging (BLI) was used to semi-quantitatively monitor the *in vivo* engraftment, outgrowth and distribution of the MM cell lines. Subsequently, radiotherapy and allogeneic lymphocyte infusions were used to eradicate established tumors.

Design and Methods

Animals

The animals used in this study were RAG2$^{-/-}\gamma c^{-/-}$mice[13] that were bred and housed in the specified pathogen-free breeding unit of the Central Animal Facility of the University of Utrecht. The animals were supplied with autoclaved sterilized food pellets and distilled water *ad libitum*. All animal experiments were conducted according to Institutional Guidelines after acquiring permission from the local Ethical Committee for Animal Experimentation and in accordance with current Dutch laws on animal experiments.

Cell lines and cell cultures

The human MM cell lines that we studied were U266, RPMI-8226/S (both obtained from the American Tissue Culture Collection (ATCC), UM-9 (generated in our institute)[16], LME-1[17], XG-1[18] OPM-1[19], and L-363[20]. All MM cell lines were cultured in RPMI-1640 (Gibco, Breda, The Netherlands) supplemented with 10% fetal calf serum (Integro, Zaandam, The Netherlands), 100 U/mL penicillin (Gibco), 100 μg/mL streptomycin (Gibco), and 10 μM β-mercaptoethanol (Merck, Darmstadt, Germany). The amphotropic packaging cell line Phoenix (a kind gift from Dr. G. Nolan), PG13 cell line (ATCC) and NIH-3T3 fibroblasts (ATCC) were cultured in DMEM (Gibco) supplemented with 10% fetal calf serum, 100 U/mL penicillin and 100 μg/mL streptomycin. The cultures were maintained at 37°C with 5% CO_2 in a humidified atmosphere.

Retroviral vector production

The GFP-luciferase retroviral vector encoding a fusion gene of GFP and luciferase was generated by inserting the luciferase gene from pBSSKGFP-luc[21] (kindly provided by Dr. R. Day) into the XhoI-NotI sites of LZRSpBMN-IRES-EGFP (S-001-AB provided by Dr. G. Nolan). The amphotropic Phoenix packaging cell line and the gibbon ape leukemia virus (GALV) pseudotyped cell line PG13 were transfected with the GFP-luciferase plasmid using calcium phosphate precipitation. The viral titer was 10^5 infectious virus particles per milliliter, as determined on 3T3 cells by FACS analyses of GFP expression.

Retroviral transduction of the multiple myeloma cell lines

For retroviral transduction of MM cell lines we used retronectin-coated tissue culture plates (CH-296, Takara Shuzo, Otsu, Japan) as described previously.[22] Transduction efficiencies, as assessed by FACS analysis of GFP expression, were 11-17% with GALV pseudotyped viruses (RPMI-8226/S) or amphotropic pseudotyped viruses (rest of MM cell lines). The percentage of GFP-luciferase expressing cells was increased to 85% by FACS sorting of the transduced cells. Luciferase activity was confirmed according to manufacturer's protocol (Promega, Madison, WI, USA). FACS sorted MM cells were expanded to produce the amounts necessary for the assays. Before *in vivo* transfer, the cells were analyzed for the expression of CD45, CD38, CD86 and CD138 by labeling with phycoerythrin conjugated antibodies (Becton Dickinson Biosciences, San Jose, CA, USA).

Transplantation of multiple myeloma cells into the RAG2$^{-/-}\gamma c^{-/-}$ mice

RAG2$^{-/-}\gamma c^{-/-}$ mice (age 9-14 weeks) were used in the experiments. Twenty-four hours before the injection of the freshly cultured MM cells, mice received total body irradiation (TBI; 3.0 Gy X-rays). Between 5-20×10^6 MM cells, suspended in 200 μL phosphate-buffered saline containing 0.1% bovine serum albumin (Gibco) were injected intravenously (i.v.) via the lateral tail vein. The tumor load in the mice was determined by weekly BLI measurements as described. In case of paralysis of the

hind limbs or when the mice became moribund, they were sacrificed by cervical dislocation. Cell isolates from various skeletal parts and soft tissues were analyzed using flow cytometry (FACS) for the presence of GFP$^+$ MM cells in the total nucleated cell fraction. Bone marrow was obtained by flushing the bones with RPMI1640. Single cell suspensions from the soft tissues were produced by passage through 70 μm cell strainers (Becton Dickinson). The cell concentration was determined by adding a fixed number of 4 μm beads to the single cell suspensions just prior to flow cytometry. Ten thousand events were analyzed for blood and bone marrow samples, whereas 100,000 events from the soft tissue cell suspensions were analyzed. Organs were isolated from some of the mice and fixed in 4% formalin and used for further immuno-histochemical analyses.

Bioluminescent imaging

A few minutes before BLI, the mice were anesthetized by intramuscular (i.m.) injection of 50 μL of ketamine-xylazine-atropine. One minute before imaging, the mice received an intraperitoneal (i.p.) injection of 100 μL 7.5 mM D-luciferine (i.e. 125 mg/kg) (Synchem Chemie, Kassel, Germany) and were placed in a light-tight chamber. Bioluminescence images were taken from both the ventral and the dorsal side of the mice using a cooled charge-coupled device (CCCD) camera (Roper Scientific, Princeton Instrument, Trenton, NJ, USA), fitted to a light-tight chamber and mounted with a 50 mm F1.2 Nikon lens, controlled by the Metavue software package software (Universal Imaging Corporation, Downingtown, PA, USA). The instrument is specifically designed for photon counting. The integrated light intensity of a stack of ten sequential 1-minute exposures was used to quantify the amount of light emitted by the MM cells. A low intensity visible light image was made and used to produce *overlay* images. The images were analyzed with Metamorph Imaging System software (Universal Imaging Corporation).

Histochemical analyses

Femora were fixed and decalcified in saturated EDTA for 7 days and embedded in paraffin. Five-micron thick sections were stained with hematoxylin and eosin for histological examination. The sections were labeled with anti-CD138 (Labvision, Fremont, USA) for detection of human MM cells. PowerVision Poly HRP-anti rabbit IgG (ImmunoLogic/Klinpath, Duiven, The Netherlands) was used as the secondary antibody followed by the peroxidase enzymatic reaction.

Determination of free immunoglobulin light chain levels

The levels of human free immunoglobulin light chains (FLC) were determined in undiluted cell culture supernatants and in urine samples using automated immunoassays as described previously.[23]

Tumor-load reduction by radiotherapy

To induce a temporary reduction in tumor load, mice bearing MM tumors were subjected to TBI of 6.0 Gy X-rays in week 5 after i.v. injection of 5×10^6 U266 cells. To rescue the irradiated mice from bone marrow failure, 5×10^6 syngeneic bone marrow cells were injected i.v. The effect of the TBI on the total tumor load per mouse as well as on individual foci of MM growth was monitored by BLI.

Human peripheral blood mononuclear cells and mixed lymphocyte reaction

Human peripheral blood mononuclear cells (PBMC) isolated from buffy-coats of healthy blood donors were thawed. The percentages of CD3$^+$ cells were determined by FACS analysis and the cells were then suspended in phosphate-buffered saline/0.1% human serum albumin at $5\text{-}40\times10^6$ T cells, which were injected in a volume of 0.2 mL as effector cells into the mice. To determine the reactivity against the MM cell lines, irradiated U266 and RPMI-8226/S cells were used as target cells in a ratio of 1:1. Briefly, 40,000 effector and 40,000 target cells were cultured in round-bottom 96-well plates for 6 days and pulsed with [^{3}H] thymidine for the last 18 hours.

Tumor load reduction by immunotherapy (the graft-versus-myeloma effect)

In order to induce a graft-versus-myeloma (GvM) effect, mice bearing MM tumors were injected with various doses of human PBMC at week 5, in which the BLI signal was clearly visible in the image analysis (approximately 2-fold above the lower BLI baseline). To facilitate the engraftment of human cells, resident murine macrophage function was suppressed by i.v. injection of 2-chloromethyl biphosphonate liposomes, 1 day prior to the PBMC injection. The effect of the PBMC infusions on the MM tumor load was monitored by BLI. Mice were also monitored for the development of xenogeneic graft-versus-host disease (GvHD) as described previously.[14] The diagnosis of xenogeneic GvHD was based on a combination of poor physical condition of the mice, hunched posture, ruffled fur and a body weight loss greater than 20%, and high human T-cell engraftment of >50%.

Results

Engraftment and tumor outgrowth of multiple myeloma cell lines in RAG2$^{-/-}\gamma c^{-/-}$ mice

To test the suitability of RAG2 $^{-/-}\gamma c^{-/-}$ mice for generating a useful MM murine model, seven different MM cell lines (U266, RPMI-8226/S, XG-1, L-363, UM-9, LME-1 and OPM-1) were transduced with GFP-luciferase and inoculated into the mice. The U266, RPMI-8226/S, XG-1, L-363, and UM-9 cell lines revealed similar results in terms of selective growth (survival time 7-12 weeks) in the bone marrow compartment only. The LME-1 and OPM-1 lines also showed growth in soft tissues, such as the liver and intestines (Table 1). Detailed results for two cell lines, U266 and RPMI-8226/S, are depicted in Figures 1 and 2. After i.v. injection of the mice with 5×10^6 transduced MM cells the first signs of tumor growth, i.e. areas of

luciferase activity, in the mice were detectable in the femur and/or tibia after 2 weeks, followed by additional foci of luciferase activity in the pelvic region, skull, limbs, sternum, ribs and the spinal vertebrae (Figure 1A and 1B). On average 5-15 foci of MM growth were detected per mouse; although the pattern of distribution varied, it was specific for each mouse (Figure 1A, 1B and 1C). MM growth in the vertebrae resulted in the development of hind leg paralysis in late-stage disease in about 70% of the animals and was a reason to sacrifice the mice. The non-paralyzed mice also became moribund and were sacrificed when they lost 20% of their body weight. BLI revealed no MM lesions in soft tissues such as the spleen, lung, liver, and kidneys (Figure 1C).

In the terminal stage of U266 MM growth, mice were sacrificed and from several bone and soft tissue samples cell suspensions were prepared and analyzed by FACS (10,000-100,000 cells per sample) for the presence of MM cells. All bone marrow specimens that were positive for BLI *in vivo* contained large numbers of MM cells. Very few or no MM cells were found in specimens that did not reveal BLI signals. The expression pattern of GFP, CD45, CD38, CD138 and CD86 was not changed after the *in vivo* passage (*data not shown*). For the U266-derived tumors we examined the presence of MM cells in soft tissues (Table 2). Using flow cytometry as a read-out system with a lower threshold of 0.005% we did not detect any GFP-positive cells (Table 2). Although these results do not completely exclude the presence of MM in soft tissues, they indicate that soft tissues were not the primary site for MM growth for five out of the seven cell lines that we studied. This predominant bone marrow outgrowth was also observed for RPMI-8226/S, XG-1, L-363, and UM-9 (*data not shown*), indicating that in this model MM cell homing and growth strongly resembles that occuring in human MM. Two other lines LME-1 and OPM-1 appeared to show not only medullary but also extramedullary growth (*data not shown*).

Based on sequential BLI measurements, the growth curves of U266 and RPMI-8226/S show an exponential increase of the myeloma tumor cell load over time, for the whole mouse (Figure 2A and 2B) as well as for individual foci of MM scattered throughout the bone marrow compartment (Figure 2C and 2D). The MM tumor growth could be monitored over a range of 4 log (a factor of 10,000). The mice inoculated with U266-tumors survived 13.6±2.4 weeks. The RPMI-8226/S tumors appeared to develop a little more rapidly such that animals with these tumors had a mean survival time of 7.9±0.8 weeks. The medullary and extramedullary growing cell lines LME-1 and OPM-1 behaved as more aggressive tumors and animals innoculated with these

Table 1. Outgrowth of different multiple myeloma cell lines after i.v. injection in RAG2$^{-/-}\gamma c^{-/-}$ mice.

Cell line	*N. of cells (i.v.)*	*Location*	*Experiment termination**	*Time of death mean (weeks)*
U266	5×10^6	skeleton	paralysis	13
UM-9	20×10^6	skeleton	paralysis	12
RPMI-8226/S	5×10^6	skeleton	paralysis	8
XG-1	15×10^6	skeleton	paralysis	8
L-363	5×10^6	skeleton	paralysis	8
OPM-1	5×10^6	skeleton, liver	weight loss	4
LME-1	5×10^6	skeleton, intestinal tract	weight loss	5

*Seven cell lines were transduced with the GFP-Luciferase gene, selected for GFP$^+$ cells and injected intraveneously into RAG2$^{-/-}\gamma c^{-/-}$ mice. The location of MM growth was determined by BLI during the terminal stage of MM development. * reason for sacrificing the animals; hind leg paralysis or loss of >20% of body weight*

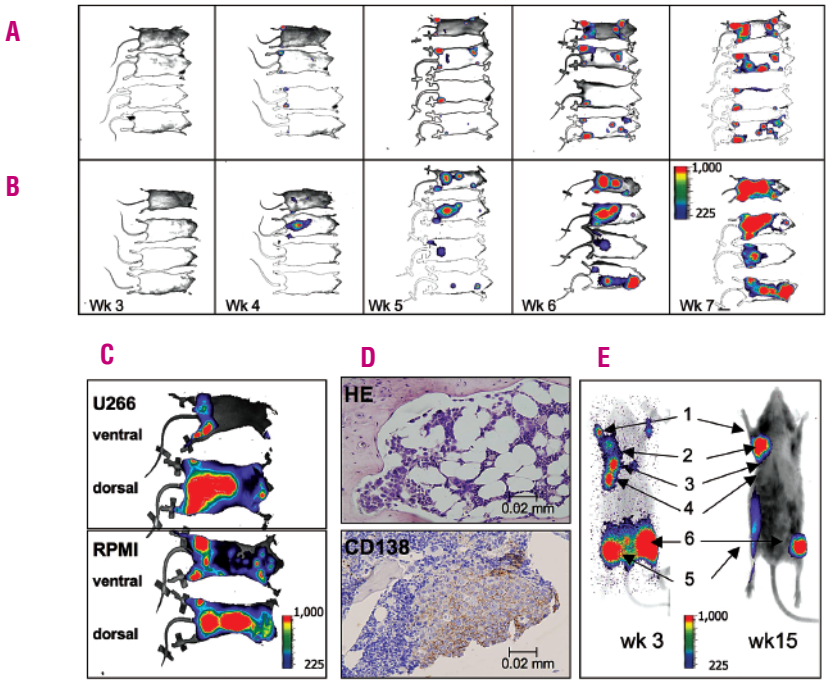

Figure 1. *In vivo* growth dynamics of luciferase gene-marked RPMI-8226/S and U266 multiple myeloma (MM). Bioluminescence images taken from the ventral side (A) or from the dorsal side (B) of the mice at five sequential time points from week 3 to 7, at 1 week intervals, after i.v. injection with GFP-Luciferase transduced RPMI-8226/S MM cells. (C) Higher magnification images taken from the dorsal and ventral sides showing distinct foci of MM growth at various sites in the bone marrow compartment of the mice inoculated with U266 or RPMI-8226/S. (D) Presence of MM cells in the bone marrow of a mouse injected with U266 shown by hematoxylin-eosin (HE) staining and by immunostaining for the expression of CD138. (E) Location of various foci of U266 MM growth before total body irradiation (week 3) and after MM re-growth measured at week 15. All images are depicted in false color, blue is at least 225 a.u./pixel and red is a maximal light intensity of 1,000 a.u./pixel.

cells survived approximately 4 to 5 weeks. In these mice the initial signs of tumor growth were in the femoral and tibial and tibia areas; soon thereafter fast growing MM tumors were observed in the liver (OPM-1) or in the abdominal (intestinal tract) region (LME-1) and in the rest of the skeleton.

Comparison of bioluminescence imaging-based and free immunoglobulin light chain-based tumor monitoring

A sensitive parameter that has been recognized as an indicator of MM burden is the concentration of FLC in the urine or plasma. *In vitro* U266 cells produce high concentrations of FLC in culture medium. We, therefore, compared the sensitivity of tumor monitoring with either BLI or urine FLC measurements in 12 mice that were inoculated with U266 cells. Whilst in all mice clearly increasing BLI-signals were observed starting from week 2 onwards, in six out of nine mice the FLC measurements remained negative until week 8 (Figure 2D), indicating that in our model BLI is a more sensitive method for monitoring the tumor load. At all time points the plasma creatine levels remained normal (*data not shown*), indicating that the measured FLC concentrations were not confounded by renal dysfunction.

Suitability of bioluminescence imaging for tumor monitoring after therapeutic interventions

To evaluate whether the newly developed MM model was suitable for sensitive tumour monitoring after therapeutic interventions, we first subjected mice bearing U266-tumors to a dose of 6.0 Gy X-rays TBI, which is the maximum tolerated dose for this strain of mouse.[22] At the time of TBI (week 5), the BLI signals were approximately 10-20 times higher than baseline level. As depicted in Figure 3A, the BLI signals in treated mice were significantly reduced to baseline levels within 2 weeks. In the meantime, the controls showed a 10-fold increase in signal. Thus, at the nadir there was a 100-fold (2 log) difference in tumor load between the treated mice and the control mice. However, BLI measurements beyond the second week after treatment revealed that, similar to the human situation, TBI was not sufficient to eradicate the MM tumors. This was evident from the steady increase of BLI signals with kinetics similar to that of the non-treated control group. These experiments demonstrated that the intervention on tumor growth in the new model was possible and that tumor regression and progression could be easily and sensitively monitored by BLI. Furthermore BLI also appeared suitable for the monitoring of individual tumor foci. A representative mouse depicted in Figure 3B and Figure 1E illustrates that, before TBI, two of the total six MM foci detected in this mouse displayed weak BLI signals. Following treatment, these two foci disappeared completely, indicating eradication of MM from the affected bones. The foci with high BLI signals, however, showed only temporary regression by TBI treatment, but eventually showed progression (Figure 3B and 1E).

Table 2. Localization of MM lesions in RAG2$^{-/-}\gamma c^{-/-}$ mice detected by bioluminescence imaging confirmed by FACS analysis.

Location	*BLI (a.u.) range*	*FACS GFP+ cells*	*MM cells detected*	*Correlation between FACS and BLI*
Skeletal parts				
femur	$1.4x10^5$-$1.5x10^7$	1.0-12.3	14/14	yes
tibia	$5.0x10^4$-$1.2x10^7$	0.8-21.8	14/14	yes
humerus	$1.2x10^5$-$9.0x10^6$	0.9-10.2	14/14	yes
sternum	BDL	< 0.01	6/7*	yes
soft tissues*				
spleen	BDL*	<0.005	0/7	yes
lungs	BDL	<0.005	0/7	yes
liver	BDL	<0.005	0/7	yes
kidney	BDL	<0.005	0/7	yes
brain	BDL	<0.005	0/7	yes
blood		<0.01	--	--

*The overall distribution of MM cells was assessed by bioluminescence imaging (BLI) in seven mice, 9 weeks after inoculation of $5x10^6$ U266 MM cells i.v. Cell isolates from various skeletal parts and soft tissues were analyzed by flow cytometry (FACS) for the presence of GFP$^+$ cells in the total nucleated cell fraction; 100,000 cells were analyzed per sample (10,000 for the blood). BLI is expressed as arbitrary light units (a.u.)/10 minutes per mouse. *: BDL: below detection limit (in region not covered by skeletal parts); *: one sternum showed a small BLI signal not confirmed by FACS analysis.*

Induction of a GvM effect in the Rag2$^{-/-}\gamma c^{-/-}$ based human myeloma model

One of our most important goals was to develop a MM model suitable for evaluation of cellular immunotherapy approaches, such as donor lymphocyte infusions (DLI). To this end, we first explored whether infusion of human

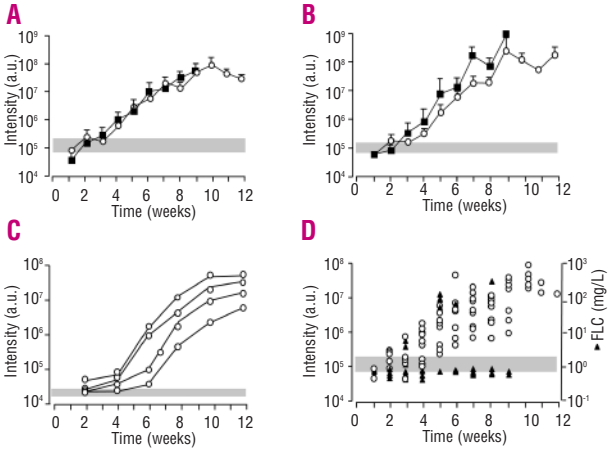

Figure 2. BLI-based growth kinetics of RPMI-8226/S and U266 multiple myeloma (MM) in RAG2 $^{-/-}\gamma c^{-/-}$ mice. MM growth curves on the basis of bioluminescence photon emission measurements with data shown as mean ± SD (n=8). The curves reflect the increase in photon emission measured for the whole mouse inoculated with RPMI-8226/S (■) or U266 MM cells (O) and imaged from the ventral side (A) and from the dorsal side (B) at various time intervals after inoculation of the MM cells. (C) Growth curves for several individual foci of bioluminescence from RPMI-8226/S in a single mouse imaged from the ventral side. (D) Comparison between levels of bioluminescence (O) and free-light-chain (FLC) (▲) concentrations recorded at several time points during MM (U266) growth. FLC were measured in the urine. The gray area at the bottom of the graphs represents the mean photon emission count from an identical sized control region in the same image over the 15 weeks.

PBMC in U266-bearing mice would induce a GvM effect. Human PBMC containing either 10×10^6 or 40×10^6 T cells were injected into mice at week 5, when the U266-tumors were clearly detectable by BLI (Figure 3C). Another group received PBMC containing 10×10^6 T cells, 1 day after the mice had been preconditioned with clodronate-containing liposomes. This preconditioning depletes murine macrophages and in our experience this improves the engraftment of human cells in the RAG2$^{-/-}\gamma c^{-/-}$ mice.[14,22] In a control group, liposomes had no anti-tumor effect (Figure 3C). As expected, all animals treated with human PBMC developed, from week 7 onwards, a cell-dose-dependent xenogeneic GVHD (*data not shown*). In mice treated with 40×10^6 T cells, the BLI signals started to drop for all tumor locations 1 week after the onset of xenogeneic GVHD. BLI signals decreased below the lower threshold levels within 2 weeks (Figure 3C). All mice were free of MM, but eventually died from lethal xenogeneic GvHD between weeks 8-12 (Table 3). At the T-cell dose of 10×10^6 (without liposome pretreatment) the xenogeneic GvHD and GvM effects were merely sufficient to stabilize the tumor progression but did not lead to tumor clearance. Only one out of six mice developed a clear xenogeneic graft-versus-host reaction. However, when combined with liposome pretreatment, 10×10^6 T cells mediated strong xenogeneic graft-versus-host and GvM effects and similar results as for the 40×10^6 T-cell group were observed. In total 31 mice were treated with PBMC from three different donors. Five animals died early from treatment-related toxicity. The remaining 26 mice all developed GvHD, although less rapidly than the group of mice that received 40×10^6 T cells; six mice died within 3 weeks, however, already with significantly reduced tumor load. The remaining 20 mice survived longer, but ultimately all died from xenogeneic GvHD between week 8 and week 12; however, these mice were all free of MM (Figure 3C and Table 3).

In our *in vitro* mixed lymphocyte reactions, the RPMI-8226/S cell line consistently failed to induce significant T-cell proliferation from PBMC of five different donors, while the U266 cell line was highly immunogenic (Figure 3D inset). The stimulation index was 697±581 for the U266 line versus 30±48 for the RPMI cell line. This suggested that RPMI-8226/S-derived tumors could represent less immunogenic MM tumors in our new model. To test this we compared the development of GvM effects against U266- or RPMI-8226/S-derived tumors in a separate experiment. Mice bearing either U266- or RPMI-8226/S tumors received PBMC containing 10×10^6 T cells 1 day after the liposome conditioning at week 5 after inoculation of the MM cells. All mice developed severe xenogeneic GvHD, and died between week 8 and 9. BLI measurements performed within this short period revealed that the GvM effect was more pronounced for the U266-tumors than for the RPMI-8226/S ones (Figure 3D). The tumor load reduction started in the U266 group at week 7, one week earlier than in the RPMI-8226/S group. At week 9, when the experiments were terminat-

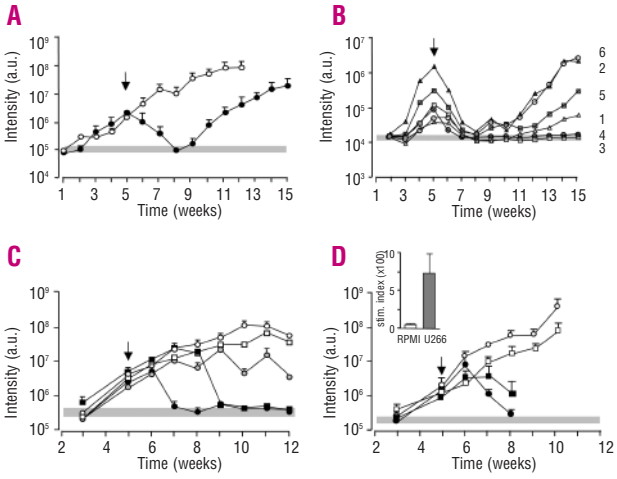

Figure 3. BLI-based monitoring of multiple myeloma (MM) tumor reduction after radiotherapy (total body irradiation) or the graft-versus-myeloma effect caused by cellular immunotherapy with human PBMC. (A) RAG2$^{-/-}\gamma^{-/-}$ mice were inoculated i.v. with U266 cells and subjected to total body irradiation in week 5 (indicated by the arrow). The MM tumor load in treated mice (●) and in non-irradiated control mice (○) was monitored weekly by BLI. The curves show the bioluminescence photon emission in arbitrary units (a.u.) for the whole mouse ± SD (n=4). (B) Individual foci of MM growth (1 through 6) in one representative mouse. The BLI images of this mouse are shown in Figure 1E and the corresponding foci of MM 1 through 6 are indicated. (C): GvM effect in mice with U266 MM cells after inoculation of 40×10^6 T cells (●) and 10×10^6 T cells (○) in week 5 (indicated by the arrow) compared to a non-treated group of mice (O). The GvM effect was also evident after inoculation of 10×10^6 T-cells in CL_2MDP liposome-pretreated mice (■) and is compared with only liposome-treated animals (■). (D). RAG2$^{-/-}\gamma^{-/-}$ mice were inoculated with 5×10^6 RPMI-8226/S or 5×10^6 U266 MM cells. At week 5 all mice were pretreated with CL2MDP liposomes followed by inoculation of 10×10^6 T cells the next day (indicated by the arrow). The GvM effect is shown in the RPMI-8226/S (■) and the U266 mice (○) compared with the non-treated RPMI-8226/S (□) and U266 mice (○). The inset bar graph shows the results of the *in vitro* mixed lymphocyte reaction analysis to RPMI-8226/S and U266 MM cells. The gray area at the bottom of the graphs represents the mean photon emission count from an identical sized control region in the same image over the 12 weeks.

Table 3. Development of xenogeneic GvHD and GvM effects in the PBMC-treated mice bearing U266-tumors.

Group	N.	TRM	x-GvHD symptoms	Cause of death x-GvHD[a]	MM[b]	MM-free[c]
Untreated MM controls	35	0	0	0	3	50
40×10^6 T cells	7	0	7	7	0	7
10×10^6 T cells	6	1	5	0	5	0
Liposomes only controls	16	6	0	0	10	0
Liposomes +10×10^6 PBMC	31	5	26	26*	0	20
Liposomes + 5×10^6 PBMC	6	1	5	4	1	0

*Data are pooled from four independent experiments with PBMC from four different individuals. Treatment: day 0: 5×10^6 MM cells; day 35: Cl2MDP-liposomes (iv); day 36 PBMC iv (on the basis of % huCD3+) as indicated. TRM: treatment-related mortality (death within 2 weeks after treatment, not GvH or MM related). [a]xenogeneic GvHD: graft-versus-host disease, i.e. severe weight loss, ruffled fur, plus high huCD45 chimerism in blood; [b]MM: high MM-associated luciferase signal plus hind leg paralysis; [c]MM-free: no MM-associated luciferase signal (BLI) *: on the basis of BLI, 20 animals were MM-free and six had substantially reduced BLI signals at the time of death.*

ed due to severe xenogeneic GvHD, the tumor load in the U266 group had almost returned to baseline levels (10±9% of starting signal), whereas the tumor load in the RPMI-8226/S group was greater (91± 53%), with the difference being statistically significant ($p<0.05$). These results suggest that RPMI-8226/S-tumors might be used as a model for non-immunogenic or DLI-resistant tumors when testing the efficacy of new combination therapies.

Discussion

In this study we present a convenient and reproducible *in vivo* model for human myeloma that can facilitate preclinical testing of cellular therapy strategies in combination with immunomodulatory agents to improve GvM effects after allogeneic stem cell transplantation. Since we aimed at convenient and sensitive immunomonitoring of tumor load, the model was established by intravenous transfer of GFP–luciferase transduced MM cell lines in RAG2$^{-/-}\gamma c^{-/-}$ mice. Despite the use of cell lines, five out of the seven tested MM cell lines produced tumors with phenotypic, dissemination, and growth patterns highly similar to those of human MM. In particular, the multifocal growth predominantly in the bone marrow, production of FLC, and expression of MM-associated molecule CD138 by the established tumors, are the most striking similarities with human MM. Furthermore, the differences in the *in vivo* growth kinetics and immunogenicity of the MM cell lines used enables us a comprehensive evaluation of novel strategies in various predefined conditions. Previously, other investigators developed MM models by injecting MM cell lines into SCID-NOD mice.[3-11] A recently developed model also exploited the advantages of fluorescence-based optical imaging, which has a high resolution for GFP imaging and also allows frequent and serial non-invasive monitoring.[28,29] While highly useful and convenient, an important drawback of this recent model was the extramedullary growth of tumors, which is not a typical feature of MM.

The mechanisms controlling the homing behavior of MM cells to the bone marrow have not yet been elucidated but it is believed that chemokines and their respective receptor counterparts involved in lymphocyte trafficking also play a role in MM homing. Differential expression of chemokine receptors has been reported for primary MM[24] as well as for MM cell lines.[25] It has been shown that SDF-1/CXCL12 is a critical regulator of MM homing.[26] Murine SDF-1, expressed by the stromal elements in mouse bone marrow, which can interact with human hematopoietic cells,[27] may play an important role in this process. Whatever the reason, extramedullary growth may introduce a significant bias, if the model is aimed at testing the efficacy of cellular immunotherapy strategies. Furthermore, outgrowth of human T cells in the SCID/NOD mice is far less reproducible than that in RAG2$^{-/-}\gamma c^{-/-}$ mice.[14] Thus, in our view, our model offers several advantages over the NOD-SCID model and may, therefore, be better suited for preclinical testing of cellular immunotherapeutic approaches. Furthermore, the availability of cell lines with different growth kinetics and with medullary or extramedullary outgrowth in our model gives us the possibility of comparing the efficacy of combination therapies in more detail. Nevertheless, it should be noted that our model, which uses cell lines rather than primary tumor cells, may be less suitable for studying a number of the biological aspects of myeloma such as stroma-myeloma interactions or natural growth kinetics. Thus far we have not tested whether RAG2$^{-/-}\gamma c^{-/-}$ immunodeficient mice facilitate the outgrowth of primary human MM cells after intravenous transfer in a similar way as has been described by other investigators who showed that primary MM cells can only engraft when injected in combination with previously implanted human fetal bone[3,10] or rabbit bone[11] fragments.

In our study, an important reason why MM cell lines were preferred to primary MM cells was to exploit the advantages of BLI as a sensitive and non-invasive technology for tumor monitoring. In our model BLI appeared superior to FLC-based monitoring and also allowed semi-quantitative monitoring of individual MM foci. Indeed, BLI appeared not only suitable for quantitative detection of the tumor load in the whole body, but it was also highly useful for visualization and quantitative analysis of individual foci of myeloma growth throughout the marrow compartment. Bioluminescence is very sensitive for the detection of low levels of marker gene expression,[30] allowing the detection of even small tumors, an aspect which becomes relevant when monitoring small tumors after therapy. Obviously, the location of the tumor (depth inside the animals) influences the lower detection limits of BLI. This is clearly seen in panel 2C for the individual foci of growth. However, once the light signals from a tumor at a given location reach levels beyond the baseline, the doubling times are similar indicating that the growth kinetics are not effected by the location. A positive correlation between tumor burden and BLI signal intensity has been shown in a variety of *in vivo* studies of animal tumor models.[30-34] We show here that this correlation also applies to the human MM cell lines that we studied and confirms reports with human MM by others.[35-37] This unique advantage enables us to evaluate the effects of therapeutic interventions on individual tumor foci, which often differ in size.

To evaluate the application areas of our model we treated established full-blown tumors with radiotherapy as well as with allogeneic cellular immunotherapy. Radiotherapy resulted in a slow decay in tumor load, initially diminishing the tumor load to below the detection limits of the BLI. Based on the whole body BLI measurements we calculated that an approximate 2 log tumor reduction was achieved by radiotherapy, which is in agreement with the radiosensitivity of the clonogenic MM cells.[38] While for small individual lesions radiotherapy seemed to be sufficient for tumor eradication (there was no reappearance of the tumor), this was clearly not the case for the larger tumor foci. Tumors in these latter foci eventually progressed at the same pace, with the radio-therapy providing only a 6- week prolongation in overall survival. These results, therefore, once again emphasize the need for additional therapies after radiotherapy. Most importantly, however, the radiotherapy experiments illustrated the feasibility of using BLI as a sensitive technology for tumor monitoring.

Finally, the results of allo-immune therapy experiments demonstrated that the MM model developed in RAG2$^{-/-}\gamma c^{-/-}$ mice is very useful for preclinical testing of cellular immune therapies, as the mice easily permit the engraftment and outgrowth of human T cells. The potent GvM effect obtained by infusion of allogeneic, thus MHC-mismatched, human T cells reveals first of all the proof of principle that it may be possible to eradicate full-blown MM by potent allo-immune cellular therapies. Secondly, the results obtained so far suggest that the cell dose and immunogenicity of myeloma cells are important parameters determining the chances of cure. While the U266-derived tumors could be completely eradicated by allo-immune treatment containing 10x10^6 T cells, the RPMI-8226/S-based tumors appeared less susceptible to the same treatment dose. Furthermore, in *in vitro* assays, the RPMI-8226/S cell line evoked little or poor responses from several HLA-mismatched PBMC. Taken together these results suggest that RPMI-8226/S-based tumors are less immunogenic than U266-derived tumors, providing us a unique opportunity to compare and optimize the efficacy of cellular immunotherapy approaches.

While at this stage we used HLA-mismatched PBMC to develop the model, it would obviously be quite interesting to evaluate the GvM effects of three locus HLA-matched PBMC which can be selected from among HLA-typed blood-bank donations. Such a model would obviously be more comparable to an HLA-identical matched unrelated donor transplantation. As mice also develop xenogeneic GvHD after infusion of human PBMC, effects on xenogeneic GvHD can be used as a control for all therapeutic interventions in combination with infusion of allogeneic lymphocytes. In this respect, we think that one interesting area of application of our current model will be the evaluation of the impact of regulatory T cells on the GvM effect, since we have recently shown in this model that co-infusion of human PBMC with autologous regulatory T cells effectively down-regulates the lethal xenogeneic GvHD.[15]

In conclusion, we present here a model of human MM growth in an immunodeficient mouse, strongly resembling human MM. This model can be used to monitor non-invasively and quantitatively the outgrowth of MM cells. It offers the possibility for preclinical evaluation of several therapeutic strategies and may, therefore, facilitate the design of optimal protocols for the treatment of MM.

Authorship and Disclosures

HR designed and performed the experiments and contributed to writing the manuscript; EvdS designed and performed the experiments and contributed to writing the manuscript; HR and EvdS contributed equally to the work described in this manuscript; LHB-B and ME performed *in vitro* experiments; VV and MCZ performed *in vitro* and *in vivo* experiments; RWG produced cell lines for this study and performed experiments; RS produced cell lines for this study and performed experiments; ACB evaluated experiments and contributed to writing the manuscipt; HML designed the research and evaluated experiments and contributed to writing the manuscipt; TM designed the research and evaluated experiments and contributed to writing the manuscipt; ACM designed the research, evaluated experiments and contributed to writing the manuscipt.

The authors reported no potential conflicts of interest.

References

1. Richardson PG, Mitsiades C, Schlossman R, Munshi N, Anderson K. New drugs for myeloma. Oncologist 2007;12:664-89.
2. Badros A, Barlogie B, Morris C, Desikan R, Martin SR, Munshi N, et al. High response rate in refractory and poor-risk multiple myeloma after allotransplantation using a non-myeloablative conditioning regimen and donor lymphocyte infusions. Blood 2001;97:2574-9.
3. Yaccoby S, Barlogie B, Epstein J. Primary myeloma cells growing in SCID-hu mice: a model for studying the biology and treatment of myeloma and its manifestations. Blood 1998;92:2908-13.
4. Pilarski LM, Hipperson G, Seeberger K, Pruski E, Coupland RW, Belch AR. Myeloma progenitors in the blood of patients with aggressive or minimal disease: engraftment and self-renewal of primary human myeloma in the bone marrow of NOD SCID mice. Blood 2000;95:1056-65.
5. Bellamy WT, Odeleye A, Finley P Huizenga B, Dalton WS, Weinstein RS, et al. An in vivo model of human multidrug-resistant multiple myeloma in SCID mice. Am J Pathol 1993; 142:691-8.
6. Urashima M, Chen BP, Chen S, Pinkus GS, Bronson RT, Dedera DA, et al. The development of a model for the homing of multiple myeloma cells to human bone marrow. Blood 1997;90:754-65.
7 Reme T, Gueydon E, Jacquet C, Klein B, Brochier J. Growth and immortalization of human myeloma cells in immunodeficient severe combined immunodeficiency mice: a preclinical model. Br J Haematol 2001;114:406-13.
8. Mitsiades C, Mitsiades N, Munshi N, Anderson KC. Focus on multiple myeloma. Cancer Cell 2004;6:439-44.
9. Huang SY, Tien HF, Su FH, Hsu SM. Nonirradiated NOD/SCID-human chimeric animal model for primary human multiple myeloma: a potential in vivo culture system. Am J Pathol 2004;164:747-56.
10. Tassone P, Neri P, Carrasco DR, Burger R, Goldmacher VS, Fram R, et al. A clinically relevant SCID-hu in vivo model of human multiple myeloma. Blood 2005;106:713-6.
11. Yata K, Yaccoby S. The SCID-rab model: a novel in vivo system for primary human myeloma demonstrating growth of CD138-expressing malignant cells. Leukemia 2004; 18:1891-7.
12. Dalton W, Anderson KC. Synopsis of a round table on validating novel therapeutics for multiple myeloma. Clin Cancer Res 2006;12:6603-10.
13. Weijer K, Uittenbogaart CH, Voordouw A, Couwenberg F, Seppen J, Blom B, et al. Intrathymic and extrathymic development of human plasmacytoid dendritic cell precursors in vivo. Blood 2002;99: 2752-9.
14. van Rijn RS, Simonetti ER, Hagenbeek A, Bonyhadi M, Storm G, Martens AC, et al. A new xenograft model for graft-versus-host disease by intravenous transfer of human peripheral blood mononuclear cells in RAG2-/- γc-/- double-mutant mice. Blood 2003;102:2522-31.
15. Mutis T, van Rijn RS, Simonetti ER, Aarts-Riemens T, Emmelot ME, van Bloois L, et al. Human regulatory T cells control xenogeneic graft-versus-host disease induced by autologous T cells in RAG2-/-γc-/- immunodeficient mice. Clin Cancer Res 2006;12: 5520-5.

16. Kuipers J, Vaandrager JW, Weghuis DO, Pearson PL, Scheres J, Lokhorst HM, et al. Fluorescence in situ hybridization analysis shows the frequent occurrence of 14q32.3 rearrangements with involvement of immunoglobulin switch regions in myeloma cell lines. Cancer Gen Cytogen 1999;109:99-107.
17. Derksen PW, Keehnen RM, Evers LM, van Oers MH, Spaargaren M, Pals ST. Cell surface proteoglycan syndecan-1 mediates hepatocyte growth factor binding and promotes Met signaling in multiple myeloma. Blood 2002;99:1405-10.
18. Zhang XG, Gaillard JP, Robillard N, Lu ZY, Gu ZJ, Jourdan M, et al. Reproducible obtaining of human myeloma cell lines as a model for tumor stem cell study in human multiple myeloma. Blood 1994;83:3654-63.
19. Katagiri S, Yonezawa T, Kuyama J, Kanayama Y, Nishida K, Abe T, et al. Two distinct human myeloma cell lines originating from one patient with myeloma. Int J Cancer 1985;36: 241-6.
20. Diehl V, Schaadt M, Kirchner H, Hellriegel KP, Gudat F, Fonatsch C, et al. Long-term cultivation of plasma cell leukemia cells and autologous lymphoblasts (LCL) in vitro: a comparative study. Blut 1978;36:331-8.
21 Day RN, Kawecki M, Berry D. Dual-function reporter protein for analysis of gene expression in living cells. Biotechniques 1998;25:848-56.
22. Rozemuller H, Knaan-Shanzer S, Hagenbeek A, van Bloois L, Storm G, Martens AC. Enhanced engraftment of human cells in RAG2/γc double-knockout mice after treatment with CL2MDP liposomes. Exp Hematol 2004;32:1118-25.
23. Abraham RS, Clark RJ, Bryant SC, Lymp JF, Larson T, Kyle RA, et al. Correlation of serum immunoglobulin free light chain quantification with urinary Bence Jones protein in light chain myeloma. Clin Chem 2002;48:655-7.
24. Möller C, Strömberg T, Juremalm M, Nilsson K, Nilsson G. Expression and function of chemokine receptors in human multiple myeloma. Leukemia 2003;17:203-10.
25. Dürig J, Schmücker U, Dührsen U. Differential expression of chemokine receptors in B cell malignancies. Leukemia 2001;15:752-6.
26. Alsayed Y, Ngo H, Runnels J, Leleu X, Singha UK, Pitsillides CM, et al. Mechanisms of regulation of CXCR4/SDF-1 (CXCL12)-dependent migration and homing in multiple myeloma. Blood 2007;109:2708-17.
27. Broxmeyer HE, Mejia JA, Hangoc G, Barese C, Dinauer M, Cooper S. SDF-1/CXCL12 enhances in vitro replating capacity of murine and human multipotential and macrophage progenitor cells. Stem Cells Dev 2007;16:589-96.
28. Mitsiades CS, Mitsiades NS, Bronson RT, Chauhan D, Munshi N, Treon SP, et al. Fluorescence imaging of multiple myeloma cells in a clinically relevant SCID/NOD in vivo model: biologic and clinical implications. Cancer Res 2003;63:6689-96.
29. Oyajobi BO, Muñoz S, Kakonen R, Williams PJ, Gupta A, Wideman CL, et al. Detection of myeloma in skeleton of mice by whole-body optical fluorescence imaging. Mol Cancer Ther 2007;6:1701-8.
30. Caceres G, Zhu XY, Jiao JA, Zankina R, Aller A, Andreotti P. Imaging of luciferase and GFP-transfected human tumours in nude mice. Luminescence 2003;18:218-23.
31. Jenkins DE, Oei Y, Hornig YS, Yu SF, Dusich J, Purchio T, Contag PR. Bioluminescent imaging (BLI) to improve and refine traditional murine models of tumor growth and metastasis. Clin Exp Metastasis 2003;20:733-44.
32 Smakman N, Martens A, Kranenburg O, Borel Rinkes IH. Validation of bioluminescence imaging of colorectal liver metastases in the mouse. J Surg Res 2004;122:225-30.
33. Paroo Z, Bollinger RA, Braasch DA, Richer E, Corey DR, Antich PP, et al. Validating bioluminescence imaging as a high-throughput, quantitative modality for assessing tumor burden. Mol Imaging 2004;3:117-24.
34. Nogawa M, Yuasa T, Kimura S, Kuroda J, Sato K, Segawa H, et al. Monitoring luciferase-labeled cancer cell growth and metastasis in different in vivo models. Cancer Lett 2005; 21:243-5.
35. Mitsiades CS, Mitsiades NS, McMullan CJ, Poulaki V, Shringarpure R, Akiyama M, et al. Inhibition of the insulin-like growth factor receptor-1 tyrosine kinase activity as a therapeutic strategy for multiple myeloma, other hematologic malignancies, and solid tumors. Cancer Cell 2004;5:221-30.
36. Wu KD, Cho YS, Katz J, Ponomarev V, Chen-Kiang S, Danishefsky SJ, et al. Investigation of antitumor effects of synthetic epothilone analogs in human myeloma models in vitro and in vivo. PNAS 2005;102:10640-5.
37. Xin X, Abrams TJ, Hollenbach PW, Rendahl KG, Tang Y, Oei YA, et al. CHIR-258 is efficacious in a newly developed fibroblast growth factor receptor 3-expressing orthotopic multiple myeloma model in mice. Clin Cancer Res 2006;12:4908-15.
38. Gluck S, Van DJ, Messner HA. Radiosensitivity of human clonogenic myeloma cells and normal bone marrow precursors: effect of different dose rates and fractionation. Int J Radiat Oncol Biol Phys 1994;28:877-82.